Check for updates

Received: 27 July 2021 | Revised: 25 October 2021 | Accepted: 3 December 2021

DOI: 10.1002/cjce.24415

ARTICLE

THE CANADIAN JOURNAL OF CHEMICAL ENGINEERING

Multivariate temporal process monitoring with graph-based predictable feature analysis

Wei Fan[1,2] | **Qinqin Zhu**[2] | **Shaojun Ren**[1] | **Bo Xu**[2] | **Fengqi Si**[1]

[1]Key Laboratory of Energy Thermal Conversion and Control of Ministry of Education, Southeast University, Nanjing, China

[2]Department of Chemical Engineering, University of Waterloo, Waterloo, Ontario, Canada

Correspondence
Qinqin Zhu, Department of Chemical Engineering, University of Waterloo, Waterloo, ON N2L 3G1, Canada.
Email: qinqin.zhu@uwaterloo.ca

Shaojun Ren, Key Laboratory of Energy Thermal Conversion and Control of Ministry of Education, Southeast University, Nanjing 210096, China.
Email: rsj@seu.edu.cn

Funding information
China Scholarship Council, Grant/Award Number: 202006090212; National Natural Science Foundation of China, Grant/Award Number: 51976031; Qinglan Project of Jiangsu Province of China; University of Waterloo

Abstract

Dynamic latent variable (DLV) methods have been widely studied for high dimensional time series monitoring by exploiting dynamic relations among process variables. However, explicit extraction of predictable information is rarely emphasized in these DLV methods. In this paper, the graph-based predictable feature analysis (GPFA) algorithm is introduced for statistical process monitoring due to its explicit predictability, and a novel index, prediction information, is designed to determine the number of its principal components for dimensionality reduction and parameter optimization. A GPFA-based dynamic process monitoring framework is proposed to differentiate among dynamic faults, normal operating condition changes, and break in relation in the normal data. Case studies on the Tennessee Eastman process and a high-pressure feedwater heater are conducted to demonstrate the superiority of GPFA over other approaches in terms of fault detection performance.

KEYWORDS

dynamic process, information theory, predictable analysis, time series monitoring

1 | INTRODUCTION

Process monitoring has received considerable attention in the past few decades, and it has played a crucial role in maintaining efficient and safe operating conditions of industrial processes.[1–6] With the ever-increasing amount of multivariate process data being collected and stored, latent variable (LV) techniques, including principal component analysis (PCA)[1,7] and partial least-squares (PLS)[8,9] have been the typical ones. They are applied to extract LV structures from collected normal data, which are further utilized to construct online monitoring frameworks. However, the assumption of time independence in PCA and PLS-based process monitoring approaches is an inherent defect.[10] Because under this assumption, process monitoring algorithms can only extract static relationships among variables. Most industrial processes have to maintain the continuity of time during dynamic control of manipulated variables. Therefore, it is inadequate to model and monitor dynamic processes with the application of static tools.

To address the dynamic modelling issues, researchers have developed several extensions of basic LV methods. Ku et al.[11] proposed a dynamic PCA (DPCA) model, which performs classical PCA on the augmented measurements with certain time lags. In other words, they attempt to derive serial correlations between current and previous observations employing settling time. After that, the fault detection indices, T^2 and squared prediction error (SPE), are calculated based on the principal component subspace (PCS) and the residual subspace (RS), respectively. Some improvements to DPCA are proposed

 © 2022 Canadian Society for Chemical Engineering.

as well,[12,13] and the number of time lags is optimized to predict the latent scores of DPCA. However, instead of focusing on the dynamic itself, the static PCA is still the main idea of DPCA. Recently, treated as an extension of PCA and PLS, canonical correlation analysis (CCA)-based methods are popular and have been successfully applied to dynamic process monitoring.[14–16] Moreover, state-space models are employed to address dynamic modelling.[17–19] When applying this kind of method, linear combinations of the past observations are treated as state variables representing dynamics. Wen et al.[20] and Ge and Chen[21] utilized a linear Gaussian state space method as dynamic latent models for process monitoring, in which expectation maximization is applied for obtaining parameters. Zhou et al.[22] improved the model from first-order dynamics to high-order dynamics, showing more general characteristics. Although the dynamic information is embodied, state-space models fail to give an explicit rank-order representation of predictability.

Recent studies have proposed several novel dynamic modelling methods, which focus more on the process dynamics instead of augmentation and state-space formulation. Dong and Qin[23] developed a dynamic inner principal component analysis (DiPCA) method for fault detection of a temporal process. They attempted to build a monitoring scheme focusing on dynamic latent variables (DLVs) that carry the most dynamic variations based on past values. However, when maximizing the covariance between DLVs and their estimates, there exists a trade-off between predictability and the variance of DLVs. A problem that cannot be ignored is that the prediction errors generated will deteriorate the accuracy of future measurements' monitoring. Wang et al.[24] put forward a forecastable component analysis (ForeCA)-based method to discover the informative structure of temporally dependent signals. ForeCA[25] is a novel dimension reduction tool, and it strives to recognize an optimal transformation to abstract the forecastable information through predictability evaluation. Though its efficiency is incredible, by analyzing the entropy in a power spectrum, the computational complexity of learning predictable features is extremely sensitive to variable dimensions. Another DLV approach, slow feature analysis (SFA),[26] was utilized to monitor operating point deviations and process dynamic anomalies.[27] Shang et al.[28] and Huang et al.[29] further adopted SFA for monitoring control performance and plant-wide process, respectively.

Despite successful applications of the above dimension reduction techniques, the field of unsupervised DLV analytics for process monitoring still has much unexplored potentiality. Motivated by SFA, Richthofer and Wiskott[30] developed predictable feature analysis (PFA). Instead of the slowest features, PFA extracts DLVs that are as predictable as possible concerning a specific prediction model. In addition, Weghenkel et al.[31] proposed a novel graph-based predictable feature analysis (GPFA) for learning dynamic information between past and future values. They combined the k-nearest neighbour (kNN) estimation and graph embedding[32] for generating predictable subspaces from time series. Another contribution of this method is that only a few assumptions of training data are needed, showing more flexibility and scalability. Mathematically, by extracting dynamic features from available observations, GPFA can predict the tendency of industrial processes. Moreover, to the best of our knowledge, GPFA has not been adapted for process monitoring purpose. It is, therefore, a promising attempt to adapt it for monitoring purpose.

In this paper, inspired by the notions of predictability, GPFA is adopted to design fault detection frameworks for dynamic processes. It aims at promoting predictions for future DLVs via utilizing dynamic latent models. With the application of GPFA, predictability measurements based on the dynamic transformations are explicitly given. It is noted that parameter selection of GPFA is an open problem. Since GPFA takes maximal predictability as the objective when trying to extract dynamic features, information theory, especially entropy,[33] is an effective technique to quantify the predictability. Therefore, an index termed predictive information[34] is adopted in this work to optimize the parameters of GPFA. Finally, the T^2 and SPE statistics are developed for monitoring the extracted dynamic and RSs, which show outstanding advantages over others. First, it gives a more generic and flexible formulation that can be easy to obtain for future extensions. Besides, only a few assumptions about training data are needed. Last but not least, integrating multi-step predictions enables an overall higher fault detection rate (FDR) and lower false alarm rate (FAR). The effectiveness of GPFA is verified through case studies on the Tennessee Eastman process (TEP) and a high-pressure feedwater heater (HPFH) with regard to fault detection performance.

The main contributions of this article are as follows:

- With only a few assumptions of temporal data, the GPFA algorithm is first adapted to design a novel framework for industrial process monitoring.
- A new index termed predictive information based on information theory is designed and utilized to select the number of principal components in GPFA.
- Two monitoring indices, T^2 and SPE, based on the obtained GPFA model are developed for process monitoring.
- Case studies of disturbances of TEP and a real fault in an HPFH are conducted, and the effectiveness of

19390019x, 2023, 2, Downloaded from https://onlinelibrary.wiley.com/doi/10.1002/cjce.24415 by East China Uni Of Sci & Tech, Wiley Online Library on [06/05/2023]. See the Terms and Conditions (https://onlinelibrary.wiley.com/terms-and-conditions) on Wiley Online Library for rules of use; OA articles are governed by the applicable Creative Commons License

GPFA is demonstrated from its comparison with several existing methods.

The rest of this paper is organized as follows. The basic algorithms of GPFA are introduced in Section 2. Section 3 proposes a method to realize dimensionality reduction of GPFA and to optimize the parameter selection. The GPFA-based process monitoring frameworks are also developed in this section. The developed frameworks are tested on the TEP and HPFH data in Sections 4 and 5, respectively. In Section 4, a thorough comparison among PCA, DiPCA, SFA, PFA, ForeCA, and GPFA is also conducted and analyzed. Finally, conclusions are drawn in Section 6.

2 | OVERVIEW OF GPFA

2.1 | The objective of GPFA

Assuming that the m-dimensional time series data $\mathbf{x}_t \in \mathbb{R}^m$ are generated by a stationary process of order p, the objective of GPFA is to find a projection subspace such that the predictability of $\mathbf{x}_t$ in the projected subspace is maximized given the past p signals.[31] In GPFA, predictability is defined to be inversely associated with the variance of the projected variables: the larger the average variance given the past p steps $[\mathbf{x}_t, \mathbf{x}_{t-1}, ..., \mathbf{x}_{t-p}]$, the lower the predictability. Mathematically, the optimization objective of GPFA is formulated as follows.[31]

Denote the input dataset $\mathbf{X}_t \in \mathbb{R}^{n\times m}$, where n is the number of collected samples. GPFA aims to find an orthogonal transformation $\mathbf{W} \in \mathbb{R}^{m\times r} = [\mathbf{w}_1, \mathbf{w}_2, ..., \mathbf{w}_r]$ such that the following expression is minimized, where r is the dimension of the feature space.

$$\min_{\mathbf{W}} \ \mathscr{L} = \mathrm{Tr}\left(\mathbb{E}_{\mathbf{S}_t^{(p)}}\left[\mathrm{cov}\left(\mathbf{S}_{t+1}|\mathbf{S}_t^{(p)}\right)\right]\right) \tag{1}$$

where $\mathbf{S}_{t+1} = \mathbf{X}_{t+1}\mathbf{W}$ is the projected variables and $\mathbf{S}_t^{(p)} = \left[\mathbf{S}_t^\top, \mathbf{S}_{t-1}^\top, ..., \mathbf{S}_{t-p}^\top\right]^\top$ is the sequential cascade of the previous k-time-step temporal series. $\mathbb{E}_{\mathbf{S}_t^{(p)}}\left[\mathrm{cov}\left(\mathbf{S}_{t+1}|\mathbf{S}_t^{(p)}\right)\right]$ denotes the expected covariance matrix of $\mathbf{S}_{t+1}$ given $\mathbf{S}_t^{(p)}$, and $\mathrm{Tr}(\cdot)$ is the trace. It is noted that in Equation (1), the sum of variances in all extracted directions is employed as a measure of the predictability of $\mathbf{S}_{t+1}$ in GPFA, and the predictability of the LV increases with the decreasing value of $\mathscr{L}$.

In practice, there might be only one $\mathbf{S}_{t+1}$ with the previous p-time-step $\mathbf{S}_t^{(p)}$, which imposes the difficulty of direct estimation of the covariance matrix $\mathrm{cov}\left(\mathbf{S}_{t+1}|\mathbf{S}_t^{(p)} = \mathbf{s}_t^{(p)}\right)$, $\left(\mathbf{s}_t^{(p)} \in \mathbb{R}^{rp}\right)$. Assuming that the conditional distribution $p\left(\mathbf{S}_{t+1}|\mathbf{S}_t^{(p)} = \mathbf{s}_t^{(p)}\right)$ can be approximated by $p\left(\mathbf{S}_{t+1}|\mathbf{S}_t^{(p)} = \mathbf{s}_t'^{(p)}\right)$ if $\mathbf{s}_t^{(p)}$ and $\mathbf{s}_t'^{(p)}$ are similar, kNN is adopted to group the most similar signals within the p past steps. It is noted that the similarity can be measured with the distance between $\mathbf{s}_t^{(p)}$ and $\mathbf{s}_t'^{(p)}$, such as Euclidean distance and Manhattan distance. In this respect, let a set $\mathcal{K}_t^{(p)}$ consist of the indices of the most similar neighbours of $\mathbf{s}_t^{(p)}$. Then Equation (1) can be adapted into the following expression.

$$\min_{\mathbf{W}} \ \mathrm{Tr}\left(\left\langle \mathrm{cov}\left(\mathbf{s}_{i+1}|i \in \mathcal{K}_t^{(p)}\right)\right\rangle_t\right) \tag{2}$$

where $\langle\cdot\rangle_t$ denotes the mean value over t. Since $\mathbf{s}_{i+1}$ and the set $\mathcal{K}_t^{(p)}$ are obtained after the transformation matrix $\mathbf{W}$ is determined, a weaker measure of the predictability is designed to be conditioned on the collected sample $\mathbf{X}_t$ instead of $\mathbf{S}_t$. Thus, Equation (2) is further simplified to

$$\min_{\mathbf{W}} \ \mathrm{Tr}\left(\left\langle \mathrm{cov}\left(\mathbf{s}_{i+1}|i \in \tilde{\mathcal{K}}_t^{(p)}\right)\right\rangle_t\right) \tag{3}$$

where $\tilde{\mathcal{K}}_t^{(p)}$ contains $\mathbf{x}_t^p$ and the indices of the k nearest neighbours of $\mathbf{x}_t$.

It has been shown that the objective of Equation (3) is equivalent to solving the following graph embedding problem.[31]

$$\begin{aligned} &\min_{\mathbf{W}} \ \sum_{i,j=1}^{k} \Theta_{ij}\left\|\mathbf{W}^\top\mathbf{x}_i - \mathbf{W}^\top\mathbf{x}_j\right\|^2 = \sum_{i,j=1}^{k}\Theta_{ij}\left\|\mathbf{s}_i - \mathbf{s}_j\right\|^2 \\ &\text{s.t.} \ \ \mathbf{W}^\top\mathbf{W} = \mathbf{I}_r \end{aligned} \tag{4}$$

where $\mathbf{I}_r$ is an r-dimensional identity matrix. $\mathbf{\Theta} \in \mathbb{R}^{k\times k}$ is a symmetric connection matrix, and its element $\Theta_{ij} = \Theta_{ji}$ represents the weight of the edges $\{\mathbf{x}_i, \mathbf{x}_j\}$ and $\{\mathbf{x}_j, \mathbf{x}_i\}$ between two connected nodes $\mathbf{x}_i$ and $\mathbf{x}_j$ from the training series. Therefore, with an appropriate selected $\mathbf{\Theta}$, the maximum predictability in the projected subspace can be achieved with the obtained transformation matrix $\mathbf{W}$ from Equation (4).

Further, denote the concatenated training series as $\mathbf{X} = [\mathbf{x}_1, \mathbf{x}_2, ..., \mathbf{x}_k] \in \mathbb{R}^{m\times k}$

$$\begin{aligned} &\mathbf{X} = [\mathbf{x}_1, \mathbf{x}_2, ..., \mathbf{x}_k] \in \mathbb{R}^{m\times k} \\ &\mathbf{D} = \mathrm{diag}\left\{\sum_j \Theta_{ij}\right\}, i = 1, 2, ..., k \\ &\mathbf{L} = \mathbf{D} - \mathbf{\Theta} \end{aligned} \tag{5}$$

19390190x, 2023, 2, Downloaded from https://onlinelibrary.wiley.com/doi/10.1002/cjce.24415 by East China Uni Of Sci & Tech, Wiley Online Library on [06/05/2023]. See the Terms and Conditions (https://onlinelibrary.wiley.com/terms-and-conditions) on Wiley Online Library for rules of use; OA articles are governed by the applicable Creative Commons License

where diag{·} denotes a diagonal matrix, and each element in $\mathbf{D} \in \mathbb{R}^{k\times k}$ is the sum of the edge coefficients linked to x_i. L is the graph Laplacian. With the denotations in Equation (5), the GPFA objective in Equation (4) can be simplified into

$$\min_{\mathbf{w}} \sum_{i=1}^{r} \mathbf{w}_i^{\top} \mathbf{X}\mathbf{L}\mathbf{X}^{\top} \mathbf{w}_i \tag{6}$$

It is noted that the objective defined in Equation (6) is equivalent to finding the r smallest eigenvectors of $\mathbf{X}\mathbf{L}\mathbf{X}^{\top}$. In the context of graph embedding, to normalize the graph embeddings, an additional constraint $\mathbf{w}_i^{\top} \mathbf{X}\mathbf{D}\mathbf{X}^{\top} \mathbf{w}_i = 1$ is added for each w_i ($i = 1, 2, ..., r$). Thereafter, the objective function in Equation (6) can be reformulated by applying the Lagrange method as follows.[35]

$$\mathscr{F} = \mathbf{w}^{\top} \mathbf{X}\mathbf{L}\mathbf{X}^{\top} \mathbf{w} - \lambda\left(\mathbf{w}^{\top} \mathbf{X}\mathbf{D}\mathbf{X}^{\top} \mathbf{w} - 1\right) \tag{7}$$

where the subscript i is omitted for better representation. Differentiating $\mathscr{F}$ with respect to w and setting it to zero lead to the following generalized eigenvalue problem

$$\mathbf{X}\mathbf{L}\mathbf{X}^{\top} \mathbf{w} = \lambda \mathbf{X}\mathbf{D}\mathbf{X}^{\top} \mathbf{w} \tag{8}$$

where λ is the smallest eigenvalue, with w being the corresponding eigenvector. It is noted that $\mathbf{X}\mathbf{L}\mathbf{X}^{\top}$ and $\mathbf{X}\mathbf{D}\mathbf{X}^{\top}$ are symmetric and positive semi-definite.[35] Thus, the optimization problem of GPFA is simplified to solve the eigenvalue problem in Equation (8).

2.2 | The GPFA algorithm

As illustrated in Section 2.1, the main idea of the GPFA algorithm is to capture the transformation matrix $\mathbf{W}$ and the latent scores $\mathbf{S}_t$. In practice, the kNN estimates $\mathcal{K}_t^{(p)}$ and the connection matrix $\mathbf{\Theta}$ becomes unreliable with increasing dimensionality of time series data. In this case, the objective in Equation (1) is unlikely the minimum. Therefore, an iterated version for improving the reliability of $\mathcal{K}_t^{(p)}$ and $\mathbf{\Theta}$ is designed. In each iteration round, the k nearest neighbours and the connection weights of the graph are continuously rebuilt until convergence is obtained or the number of iterations reaches the maximum. The detailed description of the GPFA algorithm is summarized in Algorithm 1.

ALGORITHM 1 The GPFA Algorithm

Inputs: Time series data $\mathbf{X}_t$, latent space dimensions r, time series order p, the number of k-nearest-neighbours k, and the maximum number of iterations $\boldsymbol{R}$.
Require: Preprocess $\mathbf{X}_t$ to be white according to Equation (9) and conduct the kNN algorithm on $\mathbf{X}_t$ to collect the index set $\widetilde{\mathcal{K}}_t^{(p)}$ for every sample $\mathbf{x}_t$.
Initialize $count = 0$.
repeat
  Initialize connection matrix $\mathbf{\Theta}$ as a zero matrix and construct the future graph for every $\mathbf{X}_t$, with $t = p, ..., n-1$:
  for $t = k, ..., n-1$ do
    (1) $\Theta_{i+1,j+1} \leftarrow \Theta_{i+1,j+1} + 1, \forall i,j \in \widetilde{\mathcal{K}}_t^{(k)}$ or
    (2) $\Theta_{i+1,t+1} \leftarrow \Theta_{i+1,t+1} + 1$ and $\Theta_{t+1,i+1} \leftarrow \Theta_{t+1,i+1} + 1, \forall i \in \widetilde{\mathcal{K}}_t^{(k)} \setminus \{t\}$.
  end for
  Construct the past graph for every $\mathbf{X}_t$, with $t = p+1, ..., n$:
  for $t = k+1, ..., n$ do
    (1) $\Theta_{i-k,j-k} \leftarrow \Theta_{i-k,j-k}, \forall i,j \in \widetilde{\mathcal{K}}_t^{(k)}$ or
    (2) $\Theta_{i-k,t-k} \leftarrow \Theta_{i-k,t-k} + 1$ and $\Theta_{t-k,i-k} \leftarrow \Theta_{t-k,i-k} + 1, \forall i \in \widetilde{\mathcal{K}}_t^{(k)} \setminus \{t\}$.
  end for
  Calculate $\mathbf{L}$ and $\mathbf{D}$ defined in Equation (5).
  Calculate latent scores $\mathbf{S}_t = \mathbf{X}_t\mathbf{W}$.
  Replace $\widetilde{\mathcal{K}}_t^{(k)}$ with $\mathcal{K}_t^{(k)}$, which consists of the k-nearest-neighbours of $\mathbf{S}_t^{(k)}$.
  $count \leftarrow count + 1$
until $count > \boldsymbol{R}$ or convergence
Outputs: $\mathbf{W}$ and $\mathbf{S}_t$.

19390190x, 2023, 2, Downloaded from https://onlinelibrary.wiley.com/doi/10.1002/cjce.24415 by East China Uni Of Sci & Tech, Wiley Online Library on [06/05/2023]. See the Terms and Conditions (https://onlinelibrary.wiley.com/terms-and-conditions) on Wiley Online Library for rules of use; OA articles are governed by the applicable Creative Commons License

It is noted that in GPFA the input time series data $\mathbf{X}_t$ should be whitened; otherwise, the predictability of LVs will not match the actual situation.[31] For each sample $\mathbf{x}_t$, the whitening procedure takes the following expression

$$\mathbf{x}_t^{\text{white}} = \mathbf{\Lambda}^{-1/2}\mathbf{U}^\top \mathbf{x} \tag{9}$$

where $\mathbf{\Lambda}$ contains the singular values of the covariance matrix $\mathbf{\Sigma} = \langle \mathbf{x}_t \mathbf{x}_t^\top \rangle$, and $\mathbf{U}$ is an orthogonal matrix with columns as eigenvectors of $\mathbf{\Sigma}\mathbf{\Sigma}^\top$. $\mathbf{\Lambda}$ and $\mathbf{U}$ are obtained with singular value decomposition (SVD) by $\mathbf{\Sigma} = \mathbf{U}\mathbf{\Lambda}\mathbf{U}^\top$. Cross-correlations are removed in $\mathbf{x}_t^{\text{white}}$ by sphering $\mathbf{x}_t$, and the whitened data series is then utilized as input in the GPFA algorithm.

3 | PROCESS MONITORING WITH GPFA

3.1 | Dimensionality reduction of GPFA

In the aforementioned GPFA algorithm, the latent space dimension r is an important parameter, which determines the dimension of the extracted latent space and the extent of dimensionality reduction of GPFA. Therefore, a systematic way to obtain the value of r should be designed.

Cumulative percent variance (CPV)[36] is a popular method to determine the number of principal components l in PCA, and it is calculated as

$$\text{CPV}(l) = \frac{\sum_{i=1}^{l} \lambda_i}{\sum_{i=1}^{m} \lambda_i} \times 100\% \geq \eta \tag{10}$$

where the eigenvalues $[\lambda_1, \lambda_2, ..., \lambda_m]$ of the covariance matrix are in a descending order. l is selected as the number of principal components when CPV first exceeds the control threshold η, and η determines the amount of extracted information. However, CPV is not applicable for GPFA since multiple parameters should be determined simultaneously. Additionally, their extracted predictable DLVs are not directly related with the eigenvalues $[\lambda_1, \lambda_2, ..., \lambda_m]$ in a descending order.

Alternatively, since the goal of GPFA is to maximize the predictability of their DLVs, we adopt the predictive information instead of the evaluation index.[33,37] Given a temporal series $\mathbf{X} = \{\mathbf{x}_t\}_{t=1}^n, \mathbf{x}_t \in \mathbb{R}^m$ with its probability density function (pdf) denoted as $\text{P}(\mathbf{X})$, define $\mathbf{X}_{\text{past}} = [\mathbf{x}_{t-T+1}, ..., \mathbf{x}_t]^\top$ and $\mathbf{X}_{\text{future}} = [\mathbf{x}_{t+1}, ..., \mathbf{x}_{t+T}]^\top$ as two separate consecutive series with sliding window length T. The predictive information $PI_T^{\text{pred}}(\mathbf{X})$ is designed as

$$PI_T^{\text{pred}}(\mathbf{X}) = H_T(\mathbf{X}_{\text{future}}) - H_T(\mathbf{X}_{\text{future}}|\mathbf{X}_{\text{past}}) \tag{11}$$

where $H_T(\mathbf{X}_{\text{future}})$ and $H_T(\mathbf{X}_{\text{future}}|\mathbf{X}_{\text{past}})$ represent the entropy of $\mathbf{X}_{\text{future}}$ and the conditional entropy of $\mathbf{X}_{\text{future}}$ conditioned on $\mathbf{X}_{\text{past}}$, respectively, with a window length T, which is

$$H_T(\mathbf{X}_{\text{future}}) = -\sum_{\mathbf{x}_f \in \mathbf{X}_{\text{future}}} p(\mathbf{x}_f) \log p(\mathbf{x}_f)$$

$$H_T(\mathbf{X}_{\text{future}}|\mathbf{X}_{\text{past}}) = -\sum_{\mathbf{x}_p \in \mathbf{X}_{\text{past}}} \sum_{\mathbf{x}_f \in \mathbf{X}_{\text{future}}} p(\mathbf{x}_f, \mathbf{x}_p) \log p(\mathbf{x}_f|\mathbf{x}_p)$$

where $p(\mathbf{x}_f) = \text{P}(\mathbf{X} = \mathbf{x}_f)$. With the chain rule,[38] Equation (11) can be transformed to

$$\begin{aligned} PI_T^{\text{pred}}(\mathbf{X}) &= H_T(\mathbf{X}_{\text{past}}) + H_T(\mathbf{X}_{\text{future}}) - H_T(\mathbf{X}_{\text{past}}, \mathbf{X}_{\text{future}}) \\ &= 2H_T(\mathbf{X}) - H_{2T}(\mathbf{X}) \end{aligned} \tag{12}$$

where $H(\mathbf{X}_{\text{past}}, \mathbf{X}_{\text{future}})$ is the joint entropy with length T defined as

$$H(\mathbf{X}_{\text{past}}, \mathbf{X}_{\text{future}}) = -\sum_{\mathbf{x}_p \in \mathbf{X}_{\text{past}}} \sum_{\mathbf{x}_f \in \mathbf{X}_{\text{future}}} p(\mathbf{x}_p, \mathbf{x}_f) \log p(\mathbf{x}_p, \mathbf{x}_f)$$

In GPFA, the weight matrix $\mathbf{W}$ is obtained when the predictive information in the latent scores $\mathbf{s}_t = \mathbf{W}^\top \mathbf{x}_t$ is maximized, which coincides with the definition of $PI_T^{\text{pred}}(\mathbf{S})$. To obtain the explicit expression of $PI_T^{\text{pred}}(\mathbf{S})$, inspired by the denotations in Clark et al.,[33] a spatiotemporal covariance matrix $\mathbf{\Sigma}_T(\mathbf{X})$ is defined to encode all second-order statistics of $\mathbf{X}$ across T time steps.

$$\mathbf{\Sigma}_T(\mathbf{X}) = \begin{bmatrix} C_0 & C_1 & \cdots & C_{T-1} \\ C_1^\top & C_0 & \cdots & C_{T-2} \\ \vdots & \vdots & \ddots & \vdots \\ C_{T-1}^\top & C_{T-2}^\top & \cdots & C_0 \end{bmatrix} \tag{13}$$

where $C_{\Delta t} = \langle \mathbf{x}_t \mathbf{x}_{t+\Delta t}^\top \rangle_t$. Then, the spatiotemporal covariance of S, $\mathbf{\Sigma}_T(\text{S})$, can be obtained by extending $C_{\Delta t}$ to $\mathbf{W}^\top C_{\Delta t} \mathbf{W}$, and the predictive information of DLVs is expressed as.[39]

$$PI_T^{\text{pred}}(\mathbf{S}) = 2H_T(\mathbf{S}) - H_{2T}(\mathbf{S}) = \log|\mathbf{\Sigma}_T(\mathbf{S})| - \frac{1}{2}\log|\mathbf{\Sigma}_{2T}(\mathbf{S})| \tag{14}$$

where $|\cdot|$ is the matrix determinant.

19390190x, 2023, 2, Downloaded from https://onlinelibrary.wiley.com/doi/10.1002/cjce.24415 by East China Uni Of Sci & Tech, Wiley Online Library on [06/05/2023]. See the Terms and Conditions (https://onlinelibrary.wiley.com/terms-and-conditions) on Wiley Online Library for rules of use; OA articles are governed by the applicable Creative Commons License

Therefore, $PI_T^{\text{pred}}(\mathbf{S})$ in Equation (14) is employed as the metric to select the number of DLVs r together with the time series order p and the number of nearest neighbours k. First, the range of p and k are defined, and for every $r \in [1, 2, ..., m]$, the GPFA model is developed with Algorithm 1 for each pair of (p, k) with their corresponding predictive information $PI_T^{\text{pred}}(\mathbf{S})$ calculated. The parameter set (r, p, k) with the largest $PI_T^{\text{pred}}(\mathbf{S})$ is selected as the optimal one. It is worth mentioning that the proposed parameter selection method based on predictive information is also applicable for PFA.[30]

3.2 | Monitoring statistics

Statistical indices are defined for process monitoring with reasonable assumptions, among which T^2 and SPE are the most popular ones assuming that the data follows a Gaussian distribution.[1] The T^2 statistic reflects the change of systems through the fluctuation of the LVs, while the SPE statistic represents the distance between observations and the predictable space and reflects the degree of deviation of the measurements from the model.

Given a newly measured sample $\mathbf{x}$, GPFA decomposes it into

$$\mathbf{x} = \hat{\mathbf{x}} + \tilde{\mathbf{x}} \tag{15}$$

where $\hat{\mathbf{x}} = \mathbf{W}\mathbf{W}^\top \mathbf{x}$ and $\tilde{\mathbf{x}} = (\mathbf{I}_m - \mathbf{W}\mathbf{W}^\top)\mathbf{x}$ are the projections in the DLV subspace and RS, respectively, and $\mathbf{I}_m$ is an identity matrix with dimension m. Thus, the corresponding T^2 and SPE are defined as

$$\mathrm{T}^2 = \mathbf{x}^\top \mathbf{W}\boldsymbol{\Lambda}^{-1}\mathbf{W}^\top \mathbf{x} \tag{16}$$

$$\mathrm{SPE} = \|\tilde{\mathbf{x}}\|^2 = \left\|(\mathbf{I}_m - \mathbf{W}\mathbf{W}^\top)\mathbf{x}\right\|^2 \tag{17}$$

where $\boldsymbol{\Lambda}$ is composed of selected eigenvalues for GPFA. The control limits of T^2 and SPE, denoted as ψ_{T^2} and ψ_{SPE}, are determined with the kernel density estimation (KDE), which is an effective non-parametric tool.[40,41] Using KDE, the pdf of monitoring statistics is defined as

$$f(\nu) = \frac{1}{nh}\sum_{i=1}^{n} K\left(\frac{\nu - \nu_i}{h}\right) \tag{18}$$

where h is the bandwidth parameter, ν represents the monitoring statistics, and $K(\cdot)$ is a kernel function selected as Gaussian in this paper.

With the estimated pdf, the cumulative density function is defined as

$$\mathrm{P}(\nu < \psi) = \int_{-\infty}^{\psi} f(\nu)d\nu \tag{19}$$

where the control limit ψ is obtained by setting a confidence level α, for example, 95%.

Although both T^2 and SPE are used for process monitoring in the GPFA-based monitoring scheme, it is worthwhile to point out that they represent different signals if they exceed the corresponding control limits. It is assumed that most dynamic process-relevant variations are extracted in DLV subspace, and thus it takes a much larger fault magnitude to exceed its control limit ψ_{T^2}. Further, deviations of $\mathrm{T}^2_{\text{new}}$ from ψ_{T^2} may indicate a dynamic process-relevant fault or a change in the operating conditions, which needs further investigation. On the other hand, the variations in the RS are mainly considered as noise, and its monitoring statistic SPE measures variability that breaks the normal process correlations. Thus the violation of the SPE index indicates that the variations of the sample are not consistent with the model, which should receive a higher attention.

As shown in Figure 1, the entire GPFA-based based process monitoring scheme is composed of two separate parts, namely, offline modelling and online monitoring. The goal of offline modelling is to extract the dynamic latent structure from the collected normal data with GPFA and obtain corresponding monitoring indices. For the online monitoring part, newly observed samples are transformed and detected with the trained model and predefined control limits. The detailed GPFA algorithm scheme for process monitoring is summarized as follows.

1. **Offline modelling**
   a. Preprocess collected normal $\mathbf{X}_t$ into whitened data with Equation (9);
   b. Determine model parameters r, p, and k with the method proposed in Section 3.1;
   c. Obtain the transformation matrix $\mathbf{W}$ and the latent scores $\mathbf{S}_t$ with the GPFA algorithm;
   d. Compute the control limits ψ_{T^2} and ψ_{SPE} for the DLV subspace and RS.
2. **Online monitoring**
   a. For the real-time observed sample $\mathbf{x}_{\text{new}}$, we whitened it through calculated $\boldsymbol{\Lambda}$ and $\mathbf{U}$;
   b. Obtain the monitoring statistics for $\mathrm{T}^2_{\text{new}}$ and $\mathrm{SPE}_{\text{new}}$ with Equations (16)–(17) and monitor if $\mathrm{T}^2_{\text{new}}$ or $\mathrm{SPE}_{\text{new}}$ exceeds its corresponding control limit:
      - if $\mathrm{T}^2_{\text{new}} > \psi_{\mathrm{T}^2}$, a dynamic process-relevant fault or an operating condition shift is detected with $(1-\alpha)$ confidence level;
      - if $\mathrm{SPE}_{\text{new}} > \psi_{\mathrm{SPE}}$, a fault that breaks the correlation of the GPFA model is detected with $(1-\alpha)$ confidence level;

19390190x, 2023, 2, Downloaded from https://onlinelibrary.wiley.com/doi/10.1002/cjce.24415 by East China Uni Of Sci & Tech, Wiley Online Library on [06/05/2023]. See the Terms and Conditions (https://onlinelibrary.wiley.com/terms-and-conditions) on Wiley Online Library for rules of use; OA articles are governed by the applicable Creative Commons License

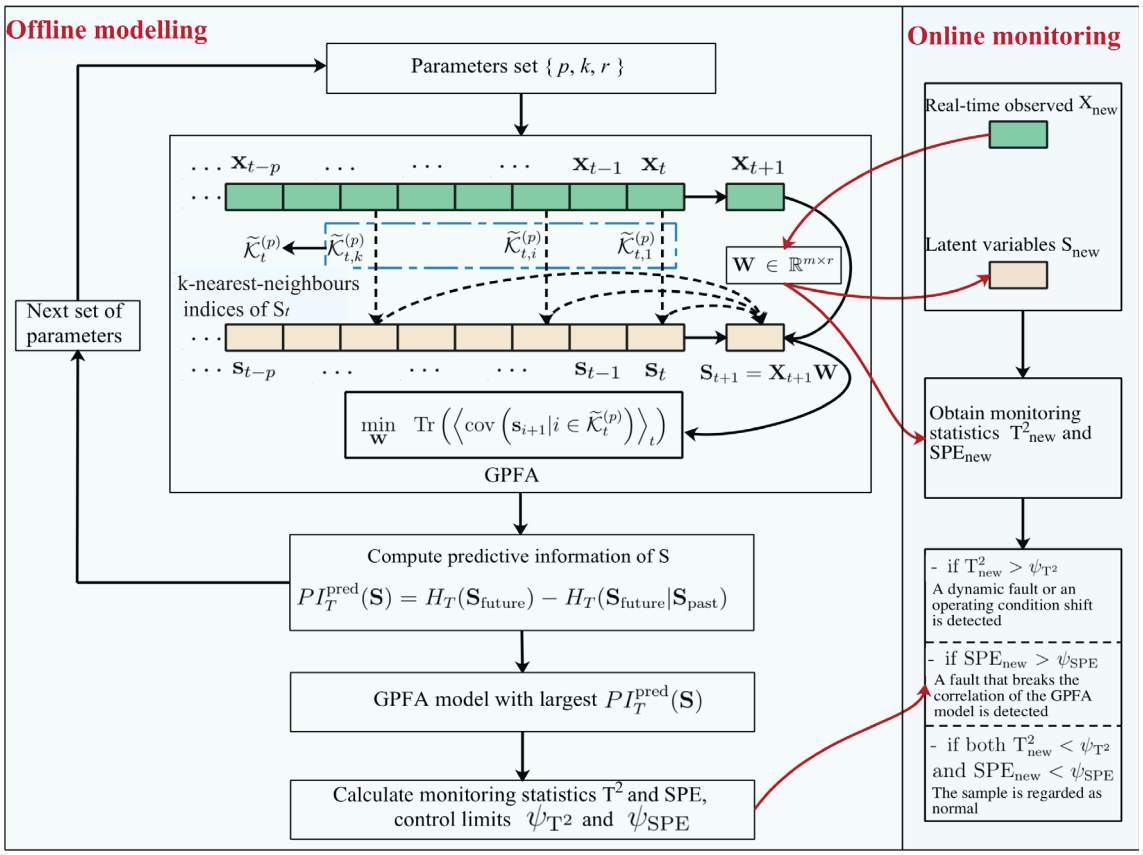

FIGURE 1 The schematic diagram of the proposed process monitoring method

- if both $T^2_{new} < \psi_{T^2}$ and $SPE_{new} < \psi_{SPE}$, the sample is regarded as normal.

4 | PROCESS MONITORING OF TEP DISTURBANCES

4.1 | Process description

The TEP is a well-established benchmark process designed to study process control strategies.[42] Two products (**G** and **H**) and a by-product (**F**) are produced from four reactants (**A**, **C**, **D**, and **E**), and the reactions are expressed as:

$$\begin{aligned}
&\mathbf{A}(\mathrm{g}) + \mathbf{C}(\mathrm{g}) + \mathbf{D}(\mathrm{g}) \rightarrow \mathbf{G}(\mathrm{liq}) \\
&\mathbf{A}(\mathrm{g}) + \mathbf{C}(\mathrm{g}) + \mathbf{E}(\mathrm{g}) \rightarrow \mathbf{H}(\mathrm{liq}) \\
&\mathbf{A}(\mathrm{g}) + \mathbf{E}(\mathrm{g}) \rightarrow \mathbf{F}(\mathrm{liq}) \\
&3\mathbf{D}(\mathrm{g}) \rightarrow 2\mathbf{F}(\mathrm{liq})
\end{aligned}$$

In total, 52 variables are involved in the TEP process, among which XMEAS (1–41) are process variables and XMV (1–11) are manipulated ones. The details of the variables are summarized in Downs and Vogel's work.[42] In our work, XMV (1–11) and XMEAS (1–22) are chosen as the input variables.

Further, 15 disturbances with known root causes (IDV [1–15]) were simulated in TEP,[42] which can be categorized into transient disturbances, persistent disturbances, and process-irrelevant disturbances based on their effect on the input variables.

4.2 | Effects of parameter selection

In this subsection, the effects of the parameters on the modelling and monitoring performance are demonstrated. The ranges of parameters are initialized as $r = [1, 2, 3, \cdots, 32, 33]$, $p = [3, 5, 7, \cdots, 27, 29]$, and $k = \{3, 5, 7, 9, 11, 13, 15\}$, and then the grid search method is conducted to search for the optimal parameters with the maximum $PI_T^{\text{pred}}(\mathbf{S})$.

The effects of different parameters on $PI_T^{\text{pred}}(\mathbf{S})$ are shown in Figure 2. It is noted that due to page limit, only a few figures are shown in this section to illustrate the effect of parameters, and other figures show similar trends. Besides, since k is the number of k-nearest-

19390019x, 2023, 2, Downloaded from https://onlinelibrary.wiley.com/doi/10.1002/cjce.24415 by East China Uni Of Sci & Tech, Wiley Online Library on [06/05/2023]. See the Terms and Conditions (https://onlinelibrary.wiley.com/terms-and-conditions) on Wiley Online Library for rules of use; OA articles are governed by the applicable Creative Commons License

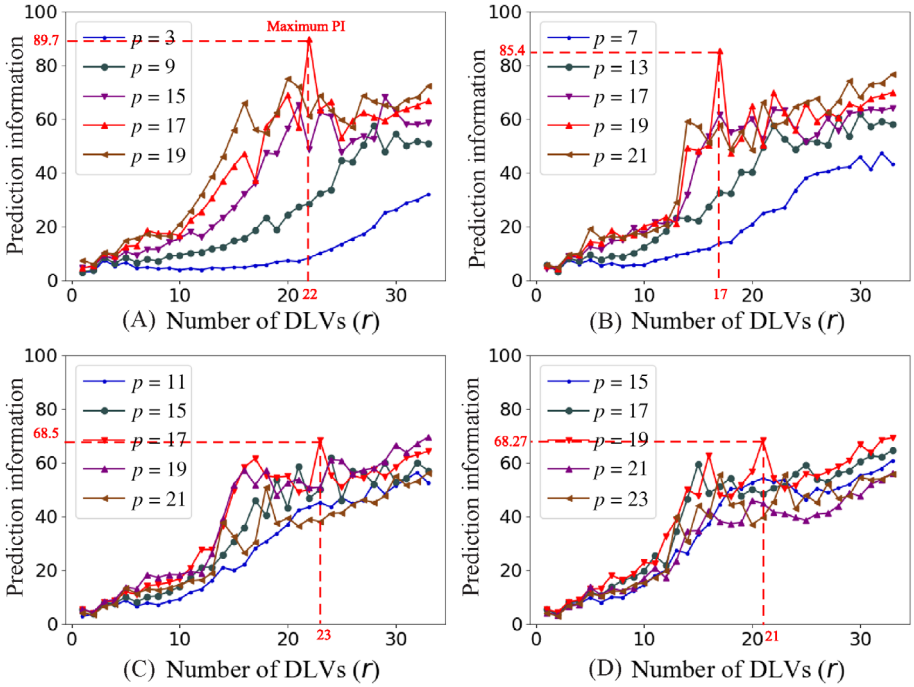

FIGURE 2 Parameter effects of the number of dynamic latent variables (DLVs) r, time series order p, and the number of nearest neighbours k for the modelling performance of graph-based predictable feature analysis (GPFA), (A) $k = 3$, (B) $k = 7$, (C) $k = 11$, and (D) $k = 15$

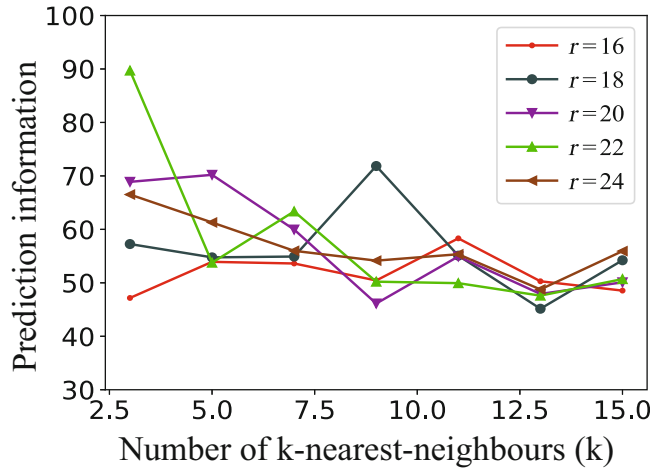

FIGURE 3 The effects of the number of nearest neighbours k and the dynamic latent variable (DLV) number r on prediction information $PI_T^{\text{pred}}(\mathbf{S})$ for fixed time series order $p = 17$

neighbour of s_t obtained from the previous p-time-step temporal series, we can conclude that k is less than or equal to p. From the figure, if k is fixed, $PI_T^{\text{pred}}(\mathbf{S})$ will increase when p increases, and at around $p = 17$, it reaches the largest value and then fluctuates below the maximum $PI_T^{\text{pred}}(\mathbf{S})$. That is, the appropriate p is located at around 17. Moreover, the number of DLVs r determines the complexity of the latent structure, and Figure 2 shows that $PI_T^{\text{pred}}(\mathbf{S})$ rises significantly first as r increases and then keeps at a relatively stable state after reaching the maximum. Figure 3 further presents the example for implementing the effects of k on $PI_T^{\text{pred}}(\mathbf{S})$ when p and r are fixed. As shown in the figure, when k takes a relatively small value (less than 10), $PI_T^{\text{pred}}(\mathbf{S})$ will reach its maximum. When p takes the remaining values, the influence of k on $PI_T^{\text{pred}}(\mathbf{S})$ shows a similar trend. It also satisfies the intuition that if k is too large, the overall similarity between the selected kNNs and the current x_t will decrease, which will reduce the effect of graph embedding. Therefore, with the parameter selection strategy proposed in Section 3.1, the optimal parameters are selected as $r = 22$, $p = 17$, and $k = 3$. The mean squared error between reconstructions $\hat{\mathbf{x}}$ and original training x given the selected parameters is 0.16, which indicates the superiority of the decomposition and reconstruction abilities of the GPFA algorithm.

To further illustrate the rationality and superiority of the prediction information-based parameter selection criterion, the fault detection rate (FDR) and false alarm rate (FAR) are employed to compare the monitoring performance with different sets of parameters. FDR and FAR are defined as follows.

$$\text{FDR} = \frac{\text{TP}}{\text{TP} + \text{FN}}$$

$$\text{FDR} = \frac{\text{FP}}{\text{FP} + \text{TN}}$$

where TP is the number of abnormal samples that are correctly detected as faults, FN is the number of wrongly classified faulty samples, FP denotes the number of

19390190x, 2023, 2, Downloaded from https://onlinelibrary.wiley.com/doi/10.1002/cjce.24415 by East China Uni Of Sci & Tech, Wiley Online Library on [06/05/2023]. See the Terms and Conditions (https://onlinelibrary.wiley.com/terms-and-conditions) on Wiley Online Library for rules of use; OA articles are governed by the applicable Creative Commons License

TABLE 1 Monitoring results of graph-based predictable feature analysis with different groups of parameters for the Tennessee Eastman process disturbances

	$k = 3, p = 17, r = 22, PI_T^{\text{pred}}(S) = 89.7$				$k = 7, p = 19, r = 17, PI_T^{\text{pred}}(S) = 85.4$			
Fault type	**T^2 (FDR)**	**T^2 (FAR)**	**SPE (FDR)**	**SPE (FAR)**	**T^2 (FDR)**	**T^2 (FAR)**	**SPE (FDR)**	**SPE (FAR)**
IDV (1)	**100.00**	1.25	99.88	1.25	99.75	**0.63**	99.88	5.00
IDV (2)	**99.75**	1.88	98.38	1.88	98.63	**1.25**	98.25	2.50
IDV (3)	**11.38**	8.13	**15.13**	8.13	2.63	6.25	12.38	8.13
IDV (4)	**100.00**	**1.25**	93.38	0.63	98.50	3.13	**99.63**	0.63
IDV (5)	**100.00**	**1.25**	**100.00**	0.63	**100.00**	3.13	**100.00**	0.63
IDV (6)	**100.00**	1.88	**100.00**	1.25	**100.00**	1.88	**100.00**	6.88
IDV (7)	**100.00**	**0.00**	99.88	2.50	**100.00**	**0.00**	**100.00**	6.88
IDV (8)	**98.50**	**0.00**	**98.13**	**1.25**	97.88	**0.00**	**98.13**	8.75
IDV (9)	**7.63**	13.13	**15.50**	8.75	4.88	**4.38**	9.75	13.75
IDV (10)	**91.00**	1.88	87.50	**1.25**	88.13	0.63	**88.00**	5.00
IDV (11)	**83.25**	3.75	70.75	2.50	74.50	0.63	**75.25**	5.63
IDV (12)	**99.88**	1.25	99.88	2.50	**99.88**	3.13	99.75	5.00
IDV (13)	**95.50**	**0.63**	95.25	1.25	**95.50**	**1.88**	95.50	2.50
IDV (14)	**100.00**	1.88	99.88	**1.25**	99.88	2.50	**100.00**	5.00
IDV (15)	**16.13**	**2.50**	13.88	**0.63**	12.25	**2.50**	16.63	5.63
Average	**80.20**	2.71	79.16	2.38	78.16	**2.13**	**79.54**	5.46
	$k = 11, p = 17, r = 23, PI_T^{\text{pred}}(S) = 68.5$				$k = 15, p = 19, r = 21, PI_T^{\text{pred}}(S) = 68.27$			
Fault type	**T^2 (FDR)**	**T^2 (FAR)**	**SPE (FDR)**	**SPE (FAR)**	**T^2 (FDR)**	**T^2 (FAR)**	**SPE (FDR)**	**SPE (FAR)**
IDV (1)	99.75	1.88	99.00	**0.63**	99.75	3.13	96.50	1.88
IDV (2)	98.75	1.88	5.63	**0.00**	98.50	**1.25**	91.38	0.63
IDV (3)	6.13	**4.38**	3.50	3.75	4.00	10.00	2.75	**2.50**
IDV (4)	98.00	3.75	94.63	0.63	72.50	2.50	99.50	**0.00**
IDV (5)	**100.00**	3.75	94.13	0.63	**100.00**	2.50	**100.00**	**0.00**
IDV (6)	**100.00**	3.13	**100.00**	0.63	**100.00**	1.88	**100.00**	**0.63**
IDV (7)	**100.00**	**0.00**	99.88	0.63	**100.00**	1.88	97.13	**0.00**
IDV (8)	98.00	1.88	52.88	**1.25**	98.00	1.88	53.00	**1.25**
IDV (9)	5.13	6.88	2.63	**1.88**	4.25	7.50	1.00	2.50
IDV (10)	86.88	3.13	74.50	**1.25**	85.00	0.63	72.38	**1.25**
IDV (11)	68.00	3.13	59.13	1.25	54.38	1.25	66.63	**0.63**
IDV (12)	**99.88**	5.00	77.25	**0.63**	**99.88**	1.25	91.75	1.25
IDV (13)	95.13	1.25	59.63	**0.00**	94.88	1.25	65.25	0.63
IDV (14)	99.88	**1.25**	**100.00**	**1.25**	99.88	**1.25**	**100.00**	**1.25**
IDV (15)	14.13	5.63	2.38	1.25	10.25	2.50	2.13	1.88
Average	77.98	3.13	61.68	**1.04**	74.75	2.71	69.29	1.08

Abbreviations: FAR, false alarm rate; FDR, fault detection rate; SPE, squared prediction error.
Note: The bold values represent the best monitoring performance for each disturbance.

incorrectly characterized normal samples, and TN represents the number of correctly identified normal samples.

In line with Figure 2, four groups of parameters are selected for comparison, and Table 1 summarizes their monitoring performances in terms of FDR and FAR. As shown in the table, with selected parameters ($k = 3$, $p = 17$, and $r = 22$), the GPFA model obtains the most maximum FDR, especially for T^2. Meanwhile, the values of FAR are kept in a reasonable range. It is noted that with parameters $k = 7$, $p = 19$, and $r = 17$, FDRs with regard to SPE indicate a better performance of GPFA. However, the corresponding FARs are larger than in

19390019x, 2023, 2, Downloaded from https://onlinelibrary.wiley.com/doi/10.1002/cjce.24415 by East China Uni Of Sci & Tech, Wiley Online Library on [06/05/2023]. See the Terms and Conditions (https://onlinelibrary.wiley.com/terms-and-conditions) on Wiley Online Library for rules of use; OA articles are governed by the applicable Creative Commons License

TABLE 2 Selected number of dynamic latent variables (DLVs) for principal component analysis (PCA), dynamic inner principal component analysis (DiPCA), slow feature analysis (SFA), predictable feature analysis (PFA), forecastable component analysis (ForeCA), and graph-based predictable feature analysis (GPFA)

Model	PCA	DiPCA	SFA	PFA	ForeCA	GPFA
No. of DLVs	19	13	55	30	59	22

TABLE 3 Fault detection rates (FDRs) comparison of principal component analysis (PCA), dynamic inner principal component analysis (DiPCA), slow feature analysis (SFA), predictable feature analysis (PFA), forecastable component analysis (ForeCA), graph-based predictable feature analysis (GPFA) for the Tennessee Eastman process (TEP) disturbances

	T^2						SPE					
Fault index	**PCA**	**DiPCA**	**SFA**	**PFA**	**ForeCA**	**GPFA**	**PCA**	**DiPCA**	**SFA**	**PFA**	**ForeCA**	**GPFA**
IDV (1)	99.75	*99.50*	99.75	*99.50*	99.88	**100.00**	**100.00**	99.88	*99.50*	*99.50*	99.88	99.88
IDV (2)	98.50	*97.88*	99.00	98.50	99.25	**99.75**	**99.75**	97.88	97.00	98.00	*95.25*	98.38
IDV (4)	89.50	56.50	85.13	*15.63*	**100.00**	**100.00**	**100.00**	99.88	*26.63*	98.75	**100.00**	93.38
IDV (5)	37.00	*32.50*	99.75	99.88	**100.00**	**100.00**	*57.38*	59.38	99.75	**100.00**	**100.00**	**100.00**
IDV (6)	99.50	*98.75*	99.75	100.00	**100.00**	**100.00**	**100.00**	*99.75*	*99.75*	**100.00**	**100.00**	**100.00**
IDV (7)	**100.00**	99.88	99.75	*71.13*	**100.00**	**100.00**	99.25	99.88	*83.63*	**99.88**	99.38	**99.88**
IDV (8)	98.13	*94.25*	**99.75**	98.88	99.25	98.50	96.50	**98.25**	*79.63*	88.63	86.88	98.13
IDV (10)	*56.00*	29.38	**97.75**	87.13	96.38	91.00	79.13	73.88	81.38	*51.75*	**88.88**	87.50
IDV (11)	71.88	62.00	**97.75**	*37.13*	89.75	83.25	78.75	**93.00**	56.88	*65.63*	79.25	70.75
IDV (12)	99.50	95.63	*78.25*	100.00	**100.00**	99.88	98.25	99.00	99.38	*96.25*	98.50	**99.88**
IDV (13)	94.88	*93.75*	**99.75**	95.88	96.13	95.50	96.13	**96.88**	*91.38*	94.13	95.75	95.25
IDV (14)	100.00	99.88	*19.63*	88.88	**100.00**	**100.00**	*93.00*	**99.88**	99.75	99.25	97.88	**99.88**
IDV (3)	*16.50*	21.88	**52.50**	33.38	38.13	11.38	18.38	**34.38**	*4.38*	9.00	*4.38*	15.13
IDV (9)	14.50	24.13	**40.75**	26.75	28.00	**7.63**	18.50	**36.63**	*3.50*	7.38	4.00	15.50
IDV (15)	*18.38*	21.88	**43.63**	31.50	36.13	16.13	23.75	**34.38**	25.13	7.25	*3.88*	13.88

Note: The values in bold represents the largest FDR among the methods, while the values in italics represent the smallest FDR.

other models, which reduces the monitoring reliability. For the remaining two groups of parameters, whose $PI_T^{\text{pred}}(\mathbf{S})$ values are less than 70, even though their overall FAR values are relatively small, the FDRs are at a low level as well, specifically for the fault detection rates with SPE. Model performances with other parameters are not presented in Table 1 due to page limit, but they can conclude from similar results that the GPFA model with higher $PI_T^{\text{pred}}(\mathbf{S})$ has better monitoring performance. Therefore, the effectiveness of the proposed parameter selection method can be verified with the consistent conclusions drawn from GPFA's monitoring performance.

4.3 | Monitoring performance comparison

To demonstrate the advantages of the proposed GPFA-based process monitoring method, it is of interest to compare detailed monitoring results of different methods (i.e., PCA, DiPCA, SFA, PFA, and ForeCA). First, the latent structures of the models are determined by cross-validation. In total, 19 principal components are selected for PCA, and for DiPCA,[23] the number of DLVs is selected as 13, and the dynamic order is 3. For SFA, according to Shang et al.,[27] the lag order is selected as 2, and the number of DLVs is chosen as 55. For PFA, via utilizing the same criterion outlined in Section 3.1, three parameters are selected as the number of DLVs $r = 30$, dynamic order $p = 5$, and error propagation index $\gamma = 3$. For ForeCA,[25] the dynamic order is selected as 2, and the number of LVs is 59. As analyzed in the above section, the parameters of GPFA are optimized as $k = 3$, $p = 17$, and $r = 22$. The designed number of DLVs of the different models is shown in Table 2.

For all models, control limits with a 99% confidence level are calculated. Thereafter, for IDV (1–15) of TEP, the overall monitoring FDRs and FARs generated by PCA, DiPCA, SFA, PFA, ForeCA, and GPFA are illustrated in Tables 3 and 4, respectively. It is observed that GPFA and

19390190x, 2023, 2, Downloaded from https://onlinelibrary.wiley.com/doi/10.1002/cjce.24415 by East China Uni Of Sci & Tech, Wiley Online Library on [06/05/2023]. See the Terms and Conditions (https://onlinelibrary.wiley.com/terms-and-conditions) on Wiley Online Library for rules of use; OA articles are governed by the applicable Creative Commons License

TABLE 4 False alarm rates (FARs) comparison of principal component analysis (PCA), dynamic inner principal component analysis (DiPCA), slow feature analysis (SFA), predictable feature analysis (PFA), forecastable component analysis (ForeCA), graph-based predictable feature analysis (GPFA) for the Tennessee Eastman process (TEP) disturbances

	T^2						SPE					
Fault index	**PCA**	**DiPCA**	**SFA**	**PFA**	**ForeCA**	**GPFA**	**PCA**	**DiPCA**	**SFA**	**PFA**	**ForeCA**	**GPFA**
IDV (1)	5.00	*19.11*	**0.00**	**0.00**	**0.00**	1.25	8.75	*34.39*	5.63	3.75	2.52	**1.25**
IDV (2)	3.13	*17.20*	**0.00**	**0.00**	**0.00**	1.88	10.00	*31.21*	2.50	4.38	6.29	**1.88**
IDV (4)	6.88	*19.11*	10.00	**0.00**	2.51	1.25	8.13	*27.39*	2.50	5.00	4.40	**0.63**
IDV (5)	6.88	*19.11*	11.25	**0.00**	2.51	1.25	8.13	*27.39*	2.50	5.00	4.40	**0.63**
IDV (6)	1.88	*11.46*	6.25	1.25	**0.00**	1.88	4.38	*23.57*	2.50	7.50	6.29	**1.25**
IDV (7)	6.25	11.46	*23.13*	20.00	11.95	**1.88**	13.75	*23.57*	1.88	6.25	**1.27**	2.50
IDV (8)	**3.75**	15.29	*33.13*	26.88	12.58	2.50	6.88	*19.11*	5.63	3.75	3.14	**1.25**
IDV (10)	6.25	*19.11*	5.00	**0.00**	1.26	1.88	11.25	*22.93*	**0.63**	7.50	3.77	1.25
IDV (11)	6.25	*24.20*	18.13	16.25	3.77	**3.75**	16.25	*27.39*	**1.88**	3.13	3.77	2.50
IDV (12)	10.00	23.57	*25.00*	23.13	16.35	**1.25**	13.75	*22.29*	3.75	5.00	2.52	**2.50**
IDV (13)	1.88	*14.65*	**0.00**	**0.00**	**0.00**	0.63	5.63	*31.21*	3.13	2.50	3.77	**1.25**
IDV (14)	7.50	19.11	*20.63*	11.88	1.89	**1.88**	6.88	*22.93*	3.13	5.00	3.14	**1.25**
IDV (3)	8.75	13.38	*45.63*	**3.13**	30.81	8.13	24.38	*26.75*	5.63	5.00	**3.14**	8.13
IDV (9)	23.13	24.84	*46.88*	35.00	38.36	**13.13**	20.63	*27.39*	6.25	6.88	**3.77**	8.75
IDV (15)	3.75	*17.83*	6.88	**0.00**	1.89	3.00	8.13	*27.39*	6.88	5.00	5.03	**0.63**

Note: The values in bold represents the smallest FAR among the methods, while the values in italics represent the largest FAR.

TABLE 5 Running time comparison of principal component analysis (PCA), dynamic inner principal component analysis (DiPCA), slow feature analysis (SFA), predictable feature analysis (PFA), forecastable component analysis (ForeCA), graph-based predictable feature analysis (GPFA) for augmented data with different time lags

	PCA		**DiPCA**		**SFA**		**PFA**		**ForeCA**		**GPFA**	
Time lags	**Train**	**Test**	**Train**	**Test**	**Train**	**Test**	**Train**	**Test**	**Train**	**Test**	**Train**	**Test**
0	0.04	0.07	0.18	0.02	0.42	0.08	0.08	0.06	537	0.23	23.15	0.08
1	0.05	0.12	0.23	0.03	0.32	0.12	0.08	0.08	4644	0.3	23.95	0.1
2	0.05	0.15	0.23	0.03	0.37	0.15	0.13	0.1	15 984	0.74	23.51	0.11
3	0.05	0.2	0.17	0.03	0.12	0.17	0.2	0.11	35 424	1.29	23.67	0.19
4	0.06	0.28	0.22	0.03	0.13	0.21	0.32	0.14	67 428	2.34	24.22	0.26
5	0.05	0.36	0.64	0.04	0.19	0.24	0.44	0.18	–	–	24.59	0.21
6	0.06	0.48	0.29	0.04	0.19	0.31	0.6	0.22	–	–	25.11	0.24
7	0.08	0.63	0.27	0.04	0.2	0.36	0.98	0.33	–	–	25.63	0.31
8	0.1	0.83	0.28	0.05	0.24	0.43	1.27	0.38	–	–	26.37	0.35
9	0.09	1.03	0.24	0.05	0.27	0.5	1.57	0.45	–	–	27.24	0.41
10	0.12	1.32	0.39	0.06	0.34	0.6	2.29	0.52	–	–	28.21	0.46
11	0.1	1.51	0.33	0.06	0.42	0.67	2.21	0.53	–	–	27.51	0.54
12	0.13	2.55	0.32	0.07	0.56	0.79	2.69	0.62	–	–	25.27	0.63
13	0.16	2.71	0.64	0.08	0.74	1.62	3.41	1.17	–	–	26.11	1.01

Note: The unit of training and testing time is second (s), and the testing time is the average running time of IDV (1–15).

ForeCA obtain the best performance for almost all disturbances, with the highest FDRs and lowest FARs. PFA and SFA also achieve satisfactory performance due to their ability to model dynamics from the processes. Among all the methods, DiPCA offers a high level of FARs, which indicates its sensitivity to noise and cumulative error. For IDV (3), IDV (9), and IDV (15), all methods show their poor performance in monitoring with lower FDRs and higher FARs since these disturbances are well controlled and thus process variables are not significantly affected.

19390019x, 2023, 2, Downloaded from https://onlinelibrary.wiley.com/doi/10.1002/cjce.24415 by East China Uni Of Sci & Tech, Wiley Online Library on [06/05/2023]. See the Terms and Conditions (https://onlinelibrary.wiley.com/terms-and-conditions) on Wiley Online Library for rules of use; OA articles are governed by the applicable Creative Commons License

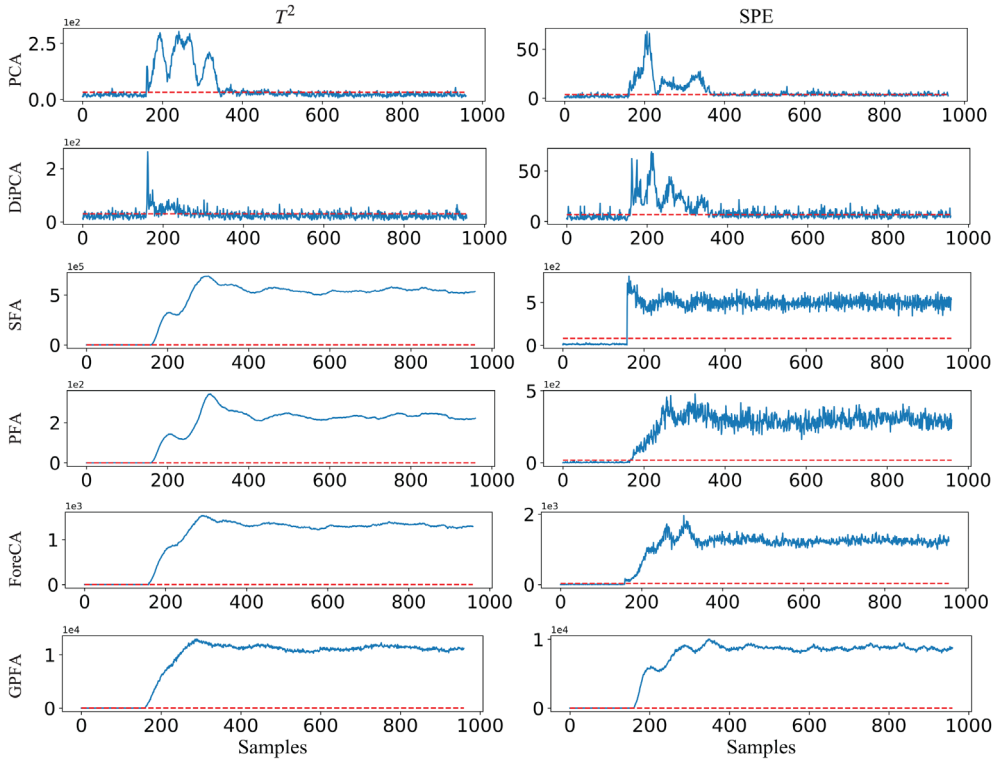

FIGURE 4 Monitoring results of IDV (5) with principal component analysis (PCA), dynamic inner principal component analysis (DiPCA), slow feature analysis (SFA), predictable feature analysis (PFA), forecastable component analysis (ForeCA), graph-based predictable feature analysis (GPFA)

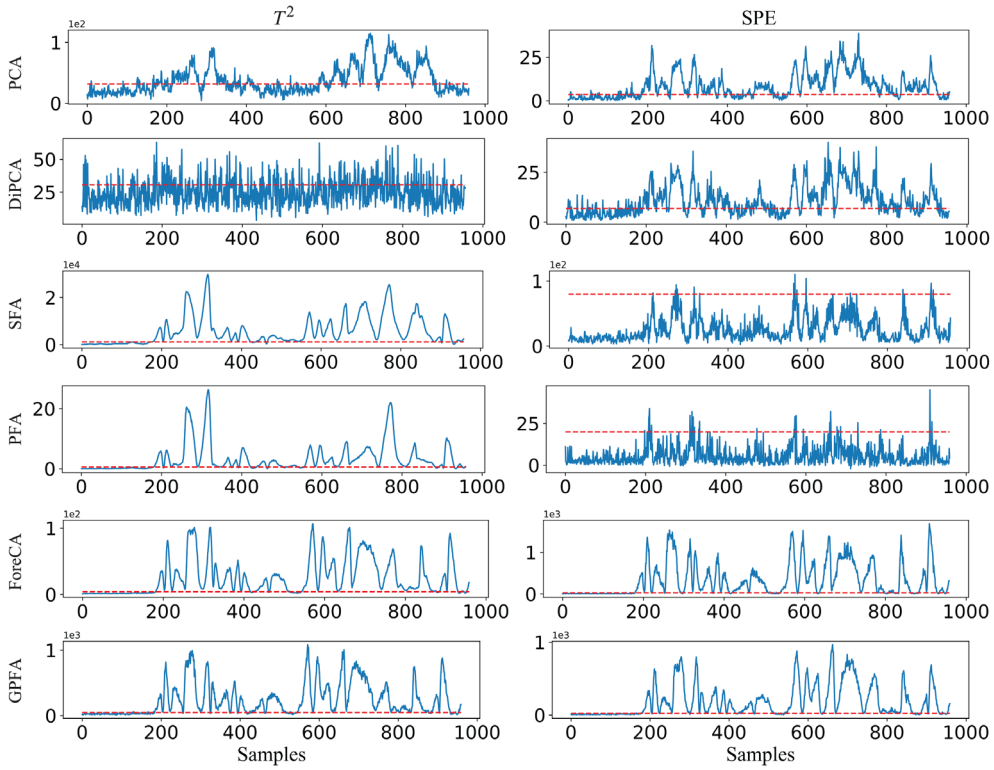

FIGURE 5 Monitoring results of IDV (10) with principal component analysis (PCA), dynamic inner principal component analysis (DiPCA), slow feature analysis (SFA), predictable feature analysis (PFA), forecastable component analysis (ForeCA), graph-based predictable feature analysis (GPFA)

Apart from monitoring performance, computing time for training is of significant importance, and the curse of dimensions should be avoided for different models. In this paper, data are augmented with past observations to evaluate the relationship between computing time and dimensions of variables, in which the dimension of input measurements M increases with time lags s with the relation $M = s \times m$. The configuration of the computational platform is specified as follows: (1) 2.4 GHz Quad-Core Intel Core i5, (2) 8 GB memory, (3) the operation system is macOS Catalina, and (4) the coding environment is Python v3.7. Table 5 depicts the running times of

19390019x, 2023, 2, Downloaded from https://onlinelibrary.wiley.com/doi/10.1002/cjce.24415 by East China Uni Of Sci & Tech, Wiley Online Library on [06/05/2023]. See the Terms and Conditions (https://onlinelibrary.wiley.com/terms-and-conditions) on Wiley Online Library for rules of use; OA articles are governed by the applicable Creative Commons License

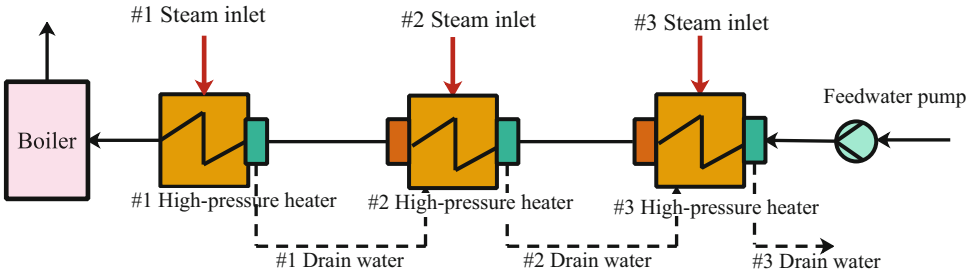

FIGURE 6 The schematic diagram of high-pressure feedwater heater group

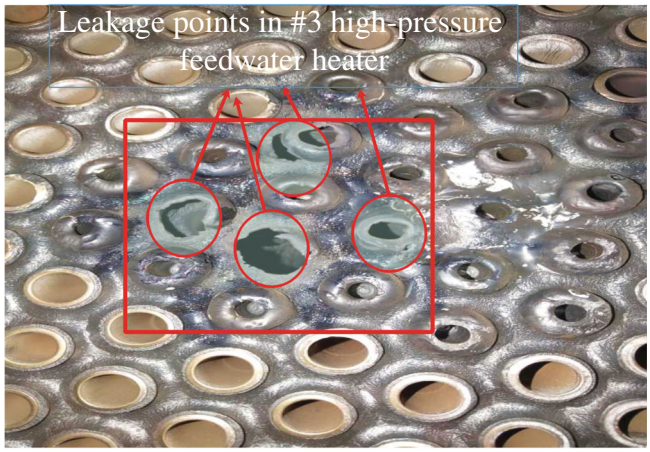

FIGURE 7 Picture of actual leakage points in #3 high-pressure feedwater heater (HPFH)

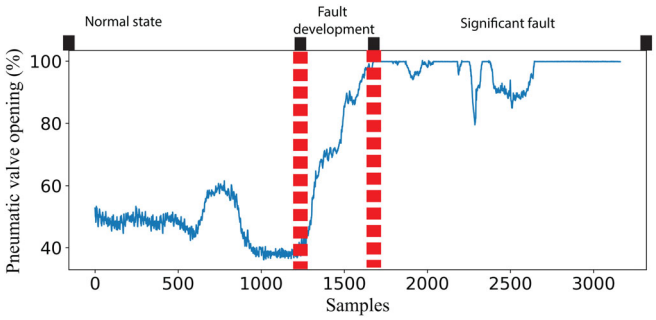

FIGURE 8 Historical variation trend of pneumatic control valve opening

different models after data augmentation. As revealed, the running times of PCA, DiPCA, SFA, PFA, and GPFA are almost invariant with respect to the input dimension, with GPFA occupying a relatively long time. However, the training time of ForeCA increases exponentially when the number of input dimensions increases, and it is easy to fall into the curse of dimensions, which is not scalable. In contrast, GPFA can achieve a good balance between computing complexity and monitoring performance. As a result, considering its superior modelling and monitoring performance, dynamic process monitoring with GPFA is the preferable option.

For better presentation of monitoring performance, two faults, IDV (5) and IDV (10), are chosen as examples for further illustration. The monitoring plots with 95% control limits of different models are shown in Figures 4 and 5, respectively, in which the blue curves represent statistics, and the red lines represent the control limits. In the case of IDV (5), a step disturbance takes place in the condenser cooling water inlet at the 161st sample. As a result, the level of the stripper decreases, and the stripper underflow is reduced. Even though with the help of adjustment to condenser cooling water flow (XMV (11)), the entire process fails to return to a stable state in a short time. Most of the stripper underflow observations from 250–300th decrease below the set-point, while the PI controller keeps adjusting to the end. As shown in Figure 4, PCA and DiPCA successfully detected the fault once the disturbance occurs. However, they fail to report the deviations of XMV (11) from the set-point after the 350th sample. In contrast, it is apparent that SFA, PFA, ForeCA, and GPFA can reveal the long-term abnormal conditions of IDV (5).

For IDV (10), a random variation occurs in the C feed temperature at the 161st sample, resulting in a change in the conditions of the stripper and the condenser. As shown in Figure 5, the random variation can be detected by all methods. However, the sensitivity of PCA, DiPCA, SFA, and PFA is low for one particular or both statistics. In comparison, ForeCA and GPFA have a better monitoring performance and are more sensitive to such random variations. In summary, considering the monitoring effect and computing complexity, our proposed GPFA-based dynamic fault monitoring framework can improve fault detection.

5 | APPLICATION IN HPFH

5.1 | Process description

The regenerative system is an essential part of thermal power plants, which plays a decisive role in the

19390191x, 2023, 2, Downloaded from https://onlinelibrary.wiley.com/doi/10.1002/cjce.24415 by East China Uni Of Sci & Tech, Wiley Online Library on [06/05/2023]. See the Terms and Conditions (https://onlinelibrary.wiley.com/terms-and-conditions) on Wiley Online Library for rules of use; OA articles are governed by the applicable Creative Commons License

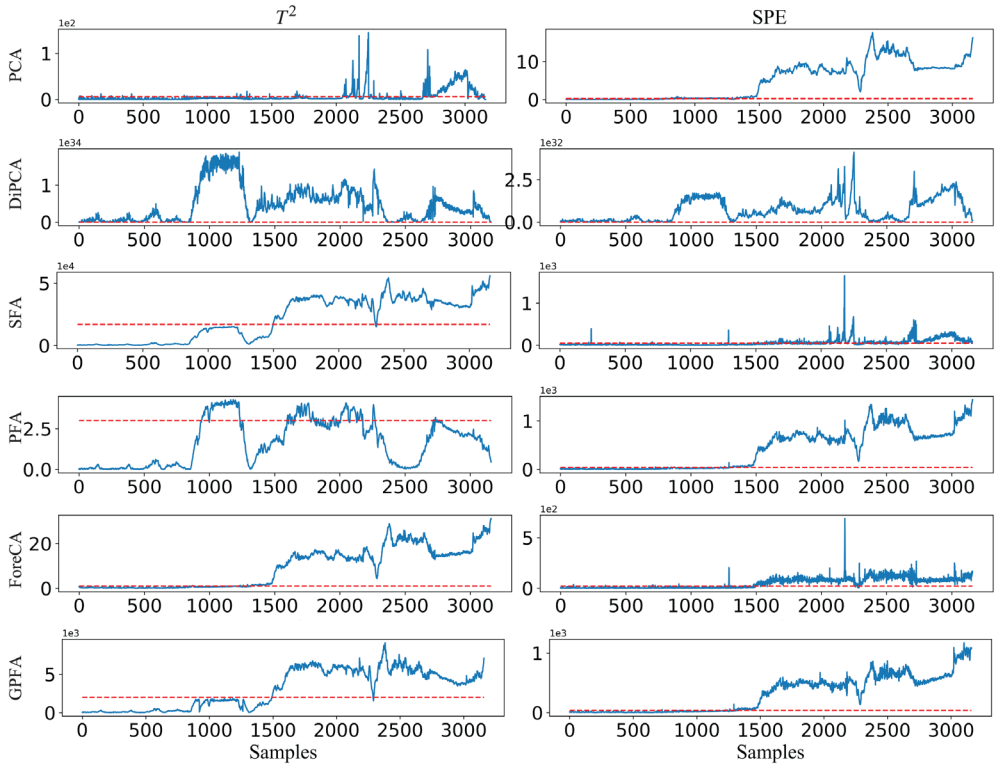

FIGURE 9 Monitoring results of #3 high-pressure feedwater heater (HPFH) with principal component analysis (PCA), dynamic inner principal component analysis (DiPCA), slow feature analysis (SFA), predictable feature analysis (PFA), forecastable component analysis (ForeCA), graph-based predictable feature analysis (GPFA)

thermal economy and safety of the unit. It consists of multiple heaters, including HPFHs, low-pressure feedwater heaters (LPFH), and a deaerator. The deaerator is a hybrid heater, and the others are surface heaters. During the regenerative process, a certain amount of steam that has done part of the work in the steam turbine is extracted to heat the condensate and feedwater. Compared with LPFH, HPFH has a harsher operating environment and a higher probability of failure. The shutdown of HPFH will cause a sharp decline in the efficiency of the unit. Therefore, accurate monitoring of HPFH is crucial in thermal power plants. The HPFH group comprises three HPFHs, as depicted in Figure 6.

In HPFH, the pressure on the waterside is far greater than the pressure on the streamside, and it is prone to leakage at the joints of the tube sheet after a long-term operation, as shown in Figure 7. When leakage occurs inside the HPFH tube bundle and the pipe cannot be blocked in time, the feedwater may enter the streamside, causing the water level to rise rapidly. A standard HPFH has three sections: a desuperheating section, a condensing section, and a drain cooler section. First of all, the superheated steam is cooled to its saturation in the desuperheating zone. In the condensing part, the energy is extracted from the steam-and-water mixture to preheat the feedwater. Finally, the drain cooler section is utilized to capture the remaining energy from the drain water.

5.2 | Experimental results and discussions

This section is based on the #3 HPFH equipped in a subcritical 300 MW coal-fired power plant. During the operation process, a leakage failure occurred in #3 HPFH. Figure 8 shows the historical variation trend of the pneumatic control valve opening of draining water (M8), which can be used to characterize the fault state. It indicates that the whole process can be separated into three stages, among which are the normal state-stage from the beginning to around the 1300th sample, the fault-developing scene between the 1300–1600th sample, and finally the significant fault stage. It is noted that the occurrence of the fault also breaks the normal relation of the input variables.

In this case study, nine operating variables, namely feedwater flow, the inlet steam pressure of #1–3 HPFH, the drain water temperature in #1–3 HPFH, pneumatic control valve opening of draining water in #3 HPFH, and the water level in #3 HPFH are selected to establish the DLV process monitoring model.[43] With a sampling interval of 60 s and a 2-day span, a total of 2880 historical measurements under normal running conditions are collected as training data. For detecting the practical fault that occurs in the #3 HPFH, PCA, DiPCA, SFA, PFA, ForeCA, and GPFA models are separately developed, and Figure 9 demonstrates their monitoring results. It is observed that both the T^2 and

19390190x, 2023, 2, Downloaded from https://onlinelibrary.wiley.com/doi/10.1002/cjce.24415 by East China Uni Of Sci & Tech, Wiley Online Library on [06/05/2023]. See the Terms and Conditions (https://onlinelibrary.wiley.com/terms-and-conditions) on Wiley Online Library for rules of use; OA articles are governed by the applicable Creative Commons License

SPE indices begin to exceed the control limit at around the 1500th sample. It is reasonable because at the beginning, when the fault occurs, the PID controller will respond quickly to make adjustments, resulting in negligible fault characteristics over time. As the disturbance insists, the controller adjustment fails, and the fault characteristics become significant. However, as shown in the figure, DiPCA cannot separate normal and faulty conditions when dealing with the #3 HPFH leakages. In addition, PCA, SFA, and PFA only have a single fault index that can accurately determine the fault, which reduces the model's reliability. Although ForeCA and GPFA have similar monitoring performance, GPFA shows a better performance in monitoring the #3 HPFH leakage fault while considering training time. In summary, the proposed GPFA monitoring framework performs great in the dynamic process monitoring of the #3 HPFH.

6 | CONCLUSIONS

In this article, a modelling and monitoring framework based on GPFA is proposed to capture the dynamic latent structure of multivariate temporal series. Since graph embedding and the conditional distribution of the data given in the previous observations are employed, GPFA can extract predictable features from multivariate temporal series. Besides, the predictive information is designed as an evaluation index for parameter optimization of GPFA. Through applications on the TEP and an HPFH process, the proposed method has shown its effectiveness over some other existing models.

This paper presents a preliminary work on dynamic process modelling and monitoring of multivariate temporal series with GPFA. For some potential future work, hybrid and probabilistic methods can be investigated to incorporate process knowledge and system randomness into modelling, respectively, to improve the prediction and anomaly detection performance. The corresponding fault diagnosis framework will also be developed for GPFA-based models to locate the root causes for detected faults.

AUTHOR CONTRIBUTIONS

Wei Fan: Conceptualization; investigation; methodology; writing – original draft. **Qinqin Zhu:** Conceptualization; funding acquisition; methodology; supervision; writing – review and editing. **Shaojun Ren:** Conceptualization; methodology; supervision; writing-review & editing. **Bo Xu:** Investigation; methodology. **Fengqi Si:** Conceptualization; methodology; supervision; writing – review and editing.

ACKNOWLEDGEMENTS

This research was supported by the China Scholarship Council (grant number: 202006090212), the Qinglan Project of Jiangsu Province of China, the National Natural Science Foundation of China (grant number: 51976031), and the University of Waterloo.

CONFLICT OF INTEREST

The authors declare no potential conflict of interests.

PEER REVIEW

The peer review history for this article is available at https://publons.com/publon/10.1002/cjce.24415.

DATA AVAILABILITY STATEMENT

The data that support the findings of this study are openly available in Tennessee Eastman Challenge Archive at https://depts.washington.edu/control/LARRY/TE/download.html, reference number 42.

REFERENCES

[1] S. Joe Qin, *J. Chemometr.* **2003**, *17*, 480.
[2] S. J. Qin, *Annu. Rev. Control* **2012**, *36*, 220.
[3] L. Zhou, Y. Wang, Z. Ge, Z. Song, *IEEE T. Ind. Inform.* **2018**, *15*, 4076.
[4] Q. Zhu, S. J. Qin, *Ind. Eng. Chem. Res.* **2019**, *58*, 11213.
[5] Z. Yang, Z. Ge, *J. Process Contr.* **2020**, *92*, 19.
[6] S. J. Qin, Y. Dong, Q. Zhu, J. Wang, Q. Liu, *Annu. Rev. Control* **2020**, *50*, 29.
[7] Q. Jiang, X. Yan, *Chemometr. Intell. Lab.* **2014**, *136*, 121.
[8] L. Gang, Q. Si-Zhao, J. Yin-Dong, Z. Dong-Hua, *Acta Automatica Sinica* **2009**, *35*, 759.
[9] Q. Zhu, S. J. Qin, Y. Dong, *Comput. Chem. Eng.* **2020**, *137*, 106809.
[10] Y. Dong, S. J. Qin, *Ind. Eng. Chem. Res.* **2020**, *59*, 2353.
[11] W. Ku, R. H. Storer, C. Georgakis, *Chemometr. Intell. Lab.* **1995**, *30*, 179.
[12] T. J. Rato, M. S. Reis, *Ind. Eng. Chem. Res.* **2013**, *52*, 13685.
[13] E. Vanhatalo, M. Kulahci, B. Bergquist, *Chemometr. Intell. Lab.* **2017**, *167*, 1.
[14] Z. Chen, S. X. Ding, K. Zhang, Z. Li, Z. Hu, *Control Eng. Pract.* **2016**, *46*, 51.
[15] Q. Jiang, F. Gao, X. Yan, H. Yi, *IEEE T. Ind. Electron.* **2018**, *66*, 3825.
[16] Q. Zhu, *J. Process Contr.* **2020**, *95*, 32.
[17] A. Negiz, A. Çlinar, *AIChE J.* **2002**, *1997*, 43.
[18] A. Negiz, A. Çinar, *J. Process Contr.* **1998**, *8*, 375.
[19] E. L. Russell, L. H. Chiang, R. D. Braatz, *Chemometr. Intell. Lab.* **2000**, *51*, 81.
[20] Q. Wen, Z. Ge, Z. Song, *AIChE J.* **2012**, *58*, 3763.
[21] Z. Ge, X. Chen, *J. Process Contr.* **2016**, *44*, 224.
[22] L. Zhou, G. Li, Z. Song, S. J. Qin, *IEEE T. Contr. Syst. T.* **2016**, *25*, 366.
[23] Y. Dong, S. J. Qin, *J. Process Contr.* **2018**, *67*, 1.
[24] D. Wang, Y. Lu, Y. Yang, *International Symposium on Computers & Informatics*, Atlantis Press, Beijing, China **2015**, p. 839.

19390019x, 2023, 2, Downloaded from https://onlinelibrary.wiley.com/doi/10.1002/cjce.24415 by East China Uni Of Sci & Tech, Wiley Online Library on [06/05/2023]. See the Terms and Conditions (https://onlinelibrary.wiley.com/terms-and-conditions) on Wiley Online Library for rules of use; OA articles are governed by the applicable Creative Commons License

[25] G. Goerg, *Proceedings of Machine Learning Research* **2013**, *28*, 64.
[26] L. Wiskott, T. J. Sejnowski, *Neural Comput.* **2002**, *14*, 715.
[27] C. Shang, F. Yang, X. Gao, X. Huang, J. A. Suykens, D. Huang, *AIChE J.* **2015**, *61*, 3666.
[28] C. Shang, B. Huang, F. Yang, D. Huang, *J. Process Contr.* **2016**, *39*, 21.
[29] J. Huang, O. K. Ersoy, X. Yan, *ISA T.* **2019**, *85*, 119.
[30] S. Richthofer, L. Wiskott, in *IEEE 14th International Conference on Machine Learning and Applications (ICMLA)*, IEEE, Miami, FL **2015**, p. 190.
[31] B. Weghenkel, A. Fischer, L. Wiskott, *Mach. Learn.* **2017**, *106*, 1359.
[32] A. N. Escalante-B, L. Wiskott, *J. Mach. Learn. Res.* **2013**, *14*, 3683.
[33] D. G. Clark, J. A. Livezey, K. E. Bouchard, ArXiv preprint **2019**, arXiv:1905.09944. https://arxiv.org/abs/1905.09944 (accessed: April 14, 2022).
[34] W. Bialek, I. Nemenman, N. Tishby, *Neural Comput.* **2001**, *13*, 2409.
[35] X. He, P. Niyogi, *Adv. Neur. In.* **2004**, *16*, 153.
[36] S. Valle, W. Li, S. J. Qin, *Ind. Eng. Chem. Res.* **1999**, *38*, 4389.
[37] S. E. Palmer, O. Marre, M. J. Berry, W. Bialek, *P. Natl. Acad. Sci. U.S.A.* **2015**, *112*, 6908.
[38] T. M. Cover, *Elements of Information Theory*, John Wiley & Sons, Hoboken, NJ **1999**.
[39] L. Li, Z. Xie, *J. Time Ser. Anal.* **1996**, *17*, 65.
[40] Z. I. Botev, J. F. Grotowski, D. P. Kroese, *Ann. Stat.* **2010**, *38*, 2916.
[41] E. Martin, A. Morris, *J. Process Contr.* **1996**, *6*, 349.
[42] J. J. Downs, E. F. Vogel, *Comput. Chem. Eng.* **1993**, *17*, 245.
[43] J. Yin, M. You, J. Cao, H. Wang, M. Tang, Y.-F. Ge, in *Databases Theory and Applications. Australasian Database Conference* (Eds: R. Borovica-Gajic, J. Qi, W. Wang), Springer, Melbourne, Australia **2020**, p. 225.

How to cite this article: W. Fan, Q. Zhu, S. Ren, B. Xu, F. Si, *Can. J. Chem. Eng.* **2023**, *101*(2), 909. https://doi.org/10.1002/cjce.24415

19390019x, 2023, 2, Downloaded from https://onlinelibrary.wiley.com/doi/10.1002/cjce.24415 by East China Uni Of Sci & Tech, Wiley Online Library on [06/05/2023]. See the Terms and Conditions (https://onlinelibrary.wiley.com/terms-and-conditions) on Wiley Online Library for rules of use; OA articles are governed by the applicable Creative Commons License